Available online at www.sciencedirect.com
ScienceDirect
European Polymer Journal 43 (2007) 3757–3765
EUROPEAN POLYMER JOURNAL
www.elsevier.com/locate/europolj

Macromolecular Nanotechnology

The effect of composition and draw-down ratio on morphology and oxygen permeability of polypropylene nanocomposite blown films

Amin Mirzadeh, Mehrdad Kokabi *

Polymer Engineering Group, Chemical Engineering Department, Faculty of Engineering, Tarbiat Modares University, P.O. Box 14115-143, Tehran, Islamic Republic of Iran

Received 6 December 2006; received in revised form 20 May 2007; accepted 10 June 2007
Available online 24 June 2007

Abstract

Polypropylene nanocomposite blown films containing organoclay were prepared by melt extrusion followed by film blowing. The effect of quantity of organically modified montmorillonite, and the compatibilizer (polypropylene-*g*-maleic anhydride, PP-*g*-MA), also the draw-down ratio on the morphology and oxygen permeability of nanocomposite films were investigated. Various characterization instruments were employed to identify the morphology, crystallinity, and dynamic mechanical properties of nanocomposite films. The oxygen permeability coefficient was evaluated based on ASTM D1434.

X-Ray diffractometry pattern for the most impermeable sample shows that the morphology of nanocomposite film is a coexistence of intercalated tactoids and exfoliated layers which is confirmed by transmission electron microscope micrographs. The results show that the oxygen permeability coefficient is influenced by the quantity of organoclay and compatibilizer, also the morphology and orientation of layered silicate.

Keywords: Polypropylene; Montmorillonite; Nanocomposite; Oxygen permeability; Blown film; Draw-down ratio

1. Introduction

Common barrier thermoplastic polymers such as polyvinylidine chloride (PVDC) and ethylene vinyl alcohol (EVOH) resin cannot be employed as monolayer due to some limitations such as processing difficulties and health care criteria. In recent years, extensive works have been carried out on production of monolayer barriers [1]. The polymer/clay nanocomposites are the best candidates for this purpose [2].

The mixing of organoclay with a polymer is mostly performed in melt state in some types of screw compounder. Intercalation and delamination (exfoliation) are two morphological characteristics related to montmorillonite layers obtained by compounding. The intercalation is the state when in the nanocomposite there are well ordered multi-layered structures with the extended polymer chains inserted into interlayers. The delaminated or exfoliated state gives a structure with separate silicate layers. Both intercalated and exfoliated structures may

* Corresponding author. Tel.: +98 21 8801 1001; fax: +98 21 8800 6544.
E-mail address: mehrir@modares.ac.ir (M. Kokabi).

0014-3057/$ - see front matter © 2007 Elsevier Ltd. All rights reserved.
doi:10.1016/j.eurpolymj.2007.06.014

be observed in a polymer matrix simultaneously [3,4].

The interactions between polymer matrix and filler particles are very important in polymer/clay nanocomposites and the surface properties play determining role in obtaining overall desirable properties [5]. Preparation of PP nanocomposites due to PP high hydrophobicity should be performed in the presence of a compatibilizer to improve the affinity of the OMMT towards polymer matrix. Currently, PP-*g*-MA has been studied and widely used in many diverse applications [6–8].

However, the presence of impermeable layers like clay in the polymer matrix can increase the tortuous path of the permeant and enhances the barrier properties. But the enhancement in these properties depends on the morphology and orientation of the clay platelets in the sample [9].

According to solution-diffusion model, for a rubbery polymer, the permeation of permeant depends on both the diffusion and the solubility of the permeant and polymer.

Polypropylene nanocomposites are multiphase systems in which the coexistence of phases with different permeabilities can create some complex transport phenomena. One can assume that transport only occurs in the permeable phase, providing one phase is permeable to the penetrant, or shows a much higher permeability compared to the other phases. In semi-crystalline polymers, the crystalline regions are considered to be gas impermeable [10], therefore, by increasing the crystallinity, the decrease in solubility attributed to amorphous volume and diffusion reduction due to more tortuous path for the diffusing molecules.

It is found that for PP and PE the solubility is proportional to the amorphous fraction [11]. Differential scanning calorimetry (DSC) is principally used to obtain a qualitative perspective on the thermal behaviour of the systems and to estimate their percentage of crystalline phase. Pukanszky et al. reported that the clay particles act as nucleating agents for the crystallization of the PP matrix and increase the crystallinity content of the matrix [12].

The crystallinity of the specimens is determined as follows:

$$\chi = \frac{\Delta H_m}{f_p \Delta H_f^0} \tag{1}$$

where ΔH_m (J/g) is the latent heat of fusion of the sample, f_p is the PP weight fraction in the sample, and ΔH_f^0 is the theoretical latent heat of fusion of a pure crystalline PP, namely 207 J/g [13].

Morphology and microstructure of nanocomposite materials are expected to play an important role in determining the transport phenomena and a higher draw-down ratio can create a more uniform nanoclay platelet orientation, leading to a more tortuous path and better barrier properties [9].

In this work, polypropylene nanocomposite blown films containing organoclay have been prepared by melt extrusion followed by film blowing and the effect of organoclay and compatibilizer quantity also the draw-down ratio on the morphology and oxygen permeability of the nanocomposite films were investigated.

2. Experimental

2.1. Materials

A commercially available polypropylene homopolymer grade (trade marked as 521P, SABIC) with a melt flow index (MFI) of 3 g/10 min (230 °C, 2.16 kg) and a density of 905 kg/m^3, was used as the base polymer.

The compatibilizer, PP grafted maleic anhydride (PP-*g*-MA) (MA content = 0.7 wt%, MFI = 200 g/10 min at 190 °C) in which maleic anhydride group is randomly grafted on a PP backbone, was purchased from Aristech, (trade marked as mp880).

Cloisite 15A**,** a natural montmorillonite modified with a quaternary ammonium salt with a cation exchange capacity of 125 meq/100 g clay (Southern Clay, Inc., USA), was used as a nanofiller.

2.2. Preparation of PP/organoclay nanocomposites

The compositions of all samples are listed in Table 1. Two master-batch consisted of PP/PP-MA/organoclay (80/10/10 wt%) and (70/20/10 wt%), namely MB1 and MB2, were melt-mixed in a Brabender dse20 co-rotating twin-screw extruder. The temperature of the extruder was maintained at 185, 190, 195, 195, 195 and 190 °C from hopper to the die and the screw speed was fixed at 150 rpm. The pellets of the master-batch were then added into PP using a ZSK twin screw extruder. The temperature in the extruder varied from 170 to 185 °C from zone 1 to zone 5 and was 180 °C in the die. The screw speed was held at 700 rpm.

Two groups of nanocomposite blown films from MB1 and MB2 were designated as F1XN.NYY and

Table 1
The composition details of the samples

Series	Sample code	PP (%)	Cloisite 15A (%)	PP-*g*-MA (%)	DDR
Master-batches	MB1	80	10	10	–
	MB2	70	10	20	–
Primary nanocomposite blown films	F1X2.505	95	2.5	2.5	5:1
	F1X2.510	95	2.5	2.5	10:1
	F1X2.515	95	2.5	2.5	15:1
	F1X2.520	95	2.5	2.5	20:1
	F1X2.525	95	2.5	2.5	25:1
Final nanocomposite blown films	F1X2.5L	95	2.5	2.5	10:1
	F1X2.5H	95	2.5	2.5	20:1
	F1X5.0L	90	5	5	10:1
	F1X5.0H	90	5	5	20:1
	F1X7.5L	85	7.5	7.5	10:1
	F1X7.5H	85	7.5	7.5	20:1
	F2X2.5L	92.5	2.5	5	10:1
	F2X2.5H	92.5	2.5	5	20:1
	F2X5.0L	85	5	10	10:1
	F2X5.0H	85	5	10	20:1
	F2X7.5L	77.5	7.5	15	10:1
	F2X7.5H	77.5	7.5	15	20:1

F2XN.NYY. In this design, N.N and YY indicate the cloisite15A percentage and magnitude of DDR, respectively. The temperature in the single extruder varied from 190 to 210 °C for zone 1 to zone 4 and was 205 °C in the die. The screw speed was kept constant.

Table 1 shows DDR of 25:1, 20:1, 15:1, 10:1, and 5:1 which were used to make primary nanocomposite blown films to investigate the effect of DDR on morphology. DDR of 10:1 and 20:1 were also selected for preparation of final nanocomposite blown films called "L" and "H" series, respectively.

2.3. Characterization

X-Ray diffraction analysis (XRD) was carried out in order to confirm whether the PP/PP-*g*-MA/Org-MMT nanocomposites were formed. The XRD patterns were scanned by X' Pert-Philips WAXS with the Cu Kα radiation ($\lambda = 0.154$ nm) operating at 40 kV and 50 mA. The angular step size was 0.2° with a step time equal to 1 s from 2° to 30° and 0.1° to 30°.

The microstructure of the nanocomposite was also examined by Zeiss CM-902a transmission electron microscope (TEM). The accelerating voltage was 80 kV.

DSC tests were carried out with a Polymer Lab in order to study the crystallinity and the possible nucleating effect of nanoclays by a ramp of 10 °C/min heating rate from −50 °C to 200 °C and a cooling step from 200 °C to 23 °C. All measurements were performed in nitrogen atmosphere.

The permeability coefficient was evaluated based on ASTM D 1434 by GDP-C instrument (Coesfeld Co.) at $23 \pm 2°$ and 35% moisture. Diffusion coefficient and solubility were calculated using time lag technique and solution-diffusion model [10].

DMTA of samples was carried out using a dynamic mechanical analyzer (242c; NETZSCH Co.) in tension mode at the following conditions: dynamic load of 2 N and static load of 10 N at frequency of 1 Hz scan rate of 2 °C/min, in the temperature range of −60 to 160 °C.

3. Results and discussion

3.1. Nanocomposite characterization

X-Ray diffraction analysis (XRD) was performed on three series of the samples as follows:

(a) Cloisite 15A and two master-batches.
(b) Primary nanocomposite blown films.
(c) Final nanocomposite blown films.

Fig. 1 shows the result of XRD analysis performed on cloisite 15A and two master-batches. As the figure shows, there are three peaks in the range of 2–10°, the first peak is related to the basal

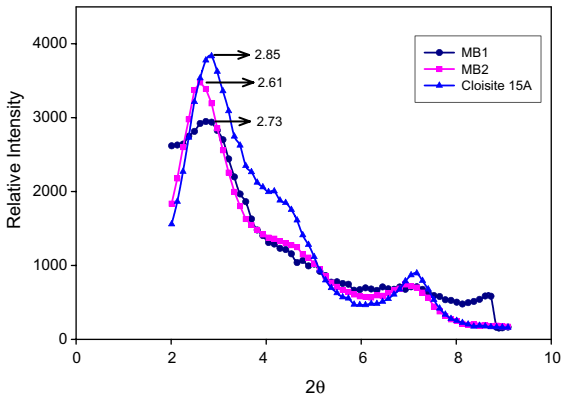

Fig. 1. XRD patterns for cloisite 15A and two made master-batches.

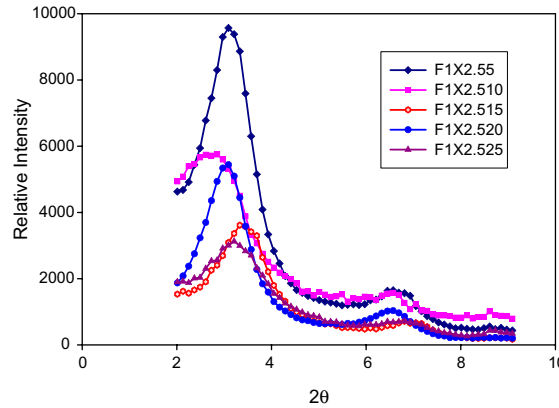

Fig. 2. XRD patterns for primary nanocomposite blown films at various draw-down ratios.

spacing (d_{001}) of the cloisite 15A which appears at $2\theta = 2.85°$ (corresponding d-spacing is 3.1 nm). The second characteristic peak of the clay is observed as a shoulder in the vicinity of the first one at $2\theta = 4.6°$ (corresponding d-spacing is 1.9 nm) and the last peak of the cloisite 15A appears at $2\theta = 7.17°$ (corresponding d-spacing is 1.1 nm) which can be attributed to the portion of the clay that is not properly modified.

In the master-batches, the above mentioned three peaks are all observed, but the d_{001} peak of the clay has been shifted to lower angle corresponding to a variation in d-spacing from 3.1 to 3.17 nm and 3.49 nm for MB1 and MB2, respectively. The higher basal spacing of clay in the MB2 in comparison with MB1 and virgin cloisite 15A (organoclay) is probably due to the higher intercalation of polymer chains inside the clay layers. It means when more PP-*g*-MA is used it makes easier the PP-*g*-MA diffusion into the organoclay layers and increases the basal spacing.

The XRD patterns of primary nanocomposite blown films show only two peaks in the range of 2–10° (Fig. 2). The corresponding d-spacing of the first one at $2\theta \cong 3.4°$ is about 2.4 nm. It may be assumed that the nanostructure is collapsed because d_{001} of cloisite 15A is 3.1 nm. This XRD pattern, in which only two peaks of three characteristic peaks of cloisite 15A is observable, is similar to the case that has been reported for PE/cloisite 15A nanocomposite by Mehrabzadeh and Kamal [14]. It has been mentioned that in such XRD pattern, there is no indication of intercalation or exfoliation and the structure is collapsed due to the shear and thermal energies. They have shown that further collapse occurs by post-processing.

At the present work, despite of observing only two characteristic peaks in Fig. 2, it is believed that the collapse of structure does not occur and the difference between primary nanocomposites blown films is merely due to the variation of draw-down ratios. Hence, the related energies are not enough to cause the structure to collapse. Therefore, in this case, it is expected to observe a peak at an angle lower than $2\theta = 2°$. To examine this matter, the final nanocomposite films were tested at very small angle, i.e. $2\theta = 0.1°$.

Fig. 3 represents the two peaks in the range of 2–10° for the first group of final nanocomposite blown films produced at low draw-down ratio (10:1). The first observed peak at $2\theta \cong 0.4°$ corresponded to d-spacing of about 2.4 nm and second peak observed at $2\theta \cong 6.5°$.

It is believed that these two peaks are related to the second and third peaks of cloisite 15A at

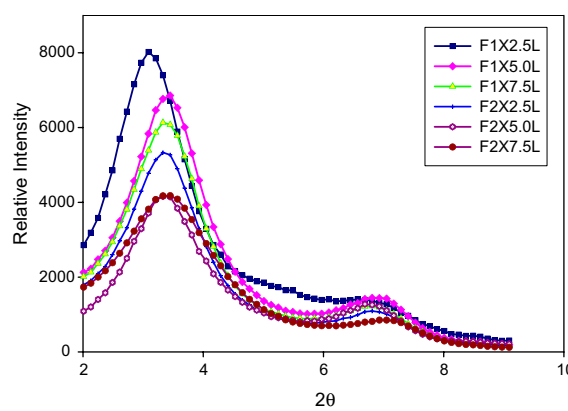

Fig. 3. XRD patterns for final nanocomposite blown films at low draw-down ratio.

$2\theta \cong 4.6°$ and $2\theta \cong 7°$, respectively. All of the peaks of cloisite 15A were shifted to the lower angle and the first one was shifted to the angle lower than $2\theta \cong 2°$. Therefore, it could not be observed by WAXD.

To overcome this problem a special setup was made [2]. This setup was comprised of a thin steel knife, a fixture and two screws. The first screw was used to align the edge of the knife with the X-ray generator and detector, while the second one was employed to adjust the position of the table in a manner to allow the sample to touch the knife. A great care was taken in adjusting the alignment of X-ray equipment, upper surface of the sample and edge of the knife. To check the setup, the XRD patterns of pure polypropylene blown films and F1X7.5H sample were recorded.

As shown in Fig. 4 there are two peaks in the range of $2\theta = 0.1–2°$. The first peak observed in this range in all the samples belongs to the noise created by instrument. However, the second peak observed at $2\theta \cong 0.8°$ (corresponding *d*-spacing is about 11 nm) is attributed to nanocomposite samples and it is related to the intercalation of polymer chains to those galleries of cloisite 15A with the original *d*-spacing of about 3.1 nm (at $2\theta \cong 2.8°$). This peak is absent in pure polypropylene.

Fig. 5 shows the XRD patterns of the nanocomposite blown film corresponding to the high draw-down ratio. According to XRD analysis which is shown in Table 2, for the best samples from morphological point of view (F1X7.5H), a coexistence of intercalated MMT tactoids and exfoliated MMT layers is observed.

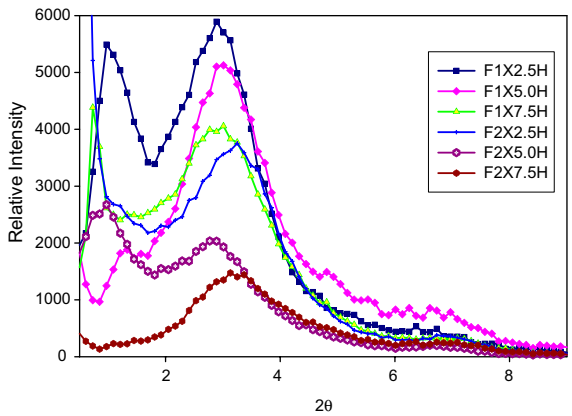

Fig. 5. XRD patterns for final nanocomposite blown films at high draw-down ratio.

Table 2
Result of XRD analysis for the final nanocomposite blown films

Sample code	Position of the peak at the angel lower than $2\theta = 2°$	Related *d*-spacing (Å)	Structure
F1X2.5	1.09	81	Intercalated
F1X5.0	1.33	66	Intercalated
F1X7.5	0.8	110	Semi exfoliated
F2X2.5	–	–	Semi-exfoliated
F2X5.0	1.09	81	Intercalated
F2X7.5	–	–	Semi-exfoliated

TEM as a complementary technique was used to evaluate the microstructure and dispersion characterization of PP/PP-*g*-MA/OMMT nanocomposite. Slides with a thickness around 70–80 nm were prepared by ultramicrotomy. TEM images of

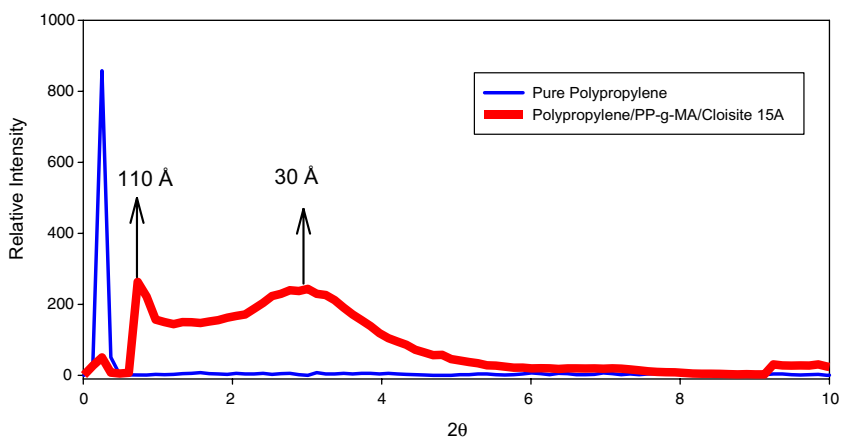

Fig. 4. XRD patterns for pure polypropylene and polypropylene nanocomposite at very small angles ($2\theta = 0.1°$).

F1X7.5H from the surface with $\vec{\theta}$ direction are shown in Fig. 6. According to these micrographs, there is a clear coexistence of intercalated MMT tactoids and exfoliated MMT layers in the sample. The oriented MMT layers along the machine direction can be clearly observed in these micrographs. This orientation is a result of draw-down ratio and orientation of polymeric chains along the machine direction.

3.2. Thermal behaviour and crystallinity

Differential scanning calorimetry was principally used to have a qualitative evaluation of the thermal behaviour of specimens and to estimate the percentage of crystalline phase in the samples. The results shown in Table 3 demonstrate that the crystallinity of the specimens of F2X group is lower than F1X group.

Although PP-*g*-MA promotes the separation of layers increasing the number of potential crystallization nuclei but this observed behaviour can be explained with the design of mixing condition. By such mixing in this work all samples could have the proper dispersion and in the samples with the same mineral content, the number of potential crystallization nuclei was approximately being equal. Using this system, the effect of PP-*g*-MA on promotion of more crystallization nuclei is decreased. Therefore, the samples with higher PP-*g*-MA/cloisite ratio showed a lower crystallinity. This idea is supported by the observed variation in T_c onset as shown in Table 3.

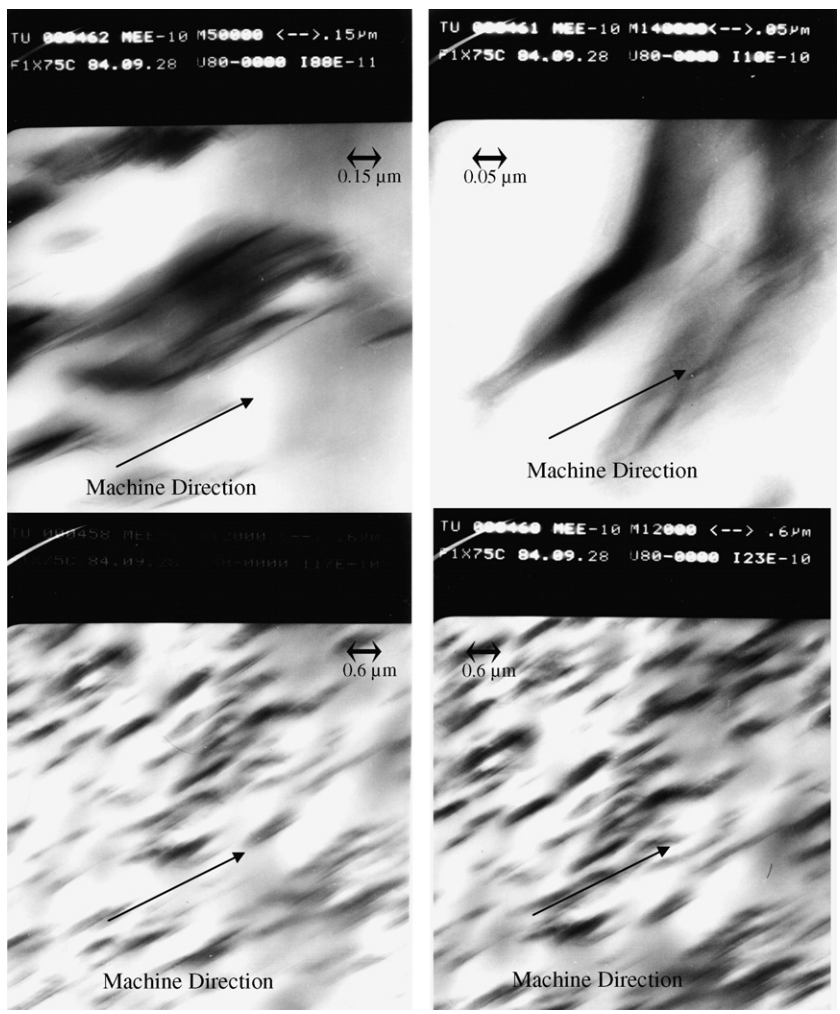

Fig. 6. TEM images of the polypropylene nanocomposite blown film at high draw-down ratio (F1X7.5H).

Table 3
DSC results of crystallinity

	Sample code	T_C (°C)	T_m (°)	Crystallinity (%)
Low draw-down ratio	PP	115	161	28.9
	F1X2.5L	121	161	34.7
	F1X5.0L	120	162	31.4
	F1X7.5L	121	160	40.4
	F2X2.5L	117	163	29.6
	F2X5.0L	119	163	23.7
	F2X7.5L	120	161	30.6
High draw-down ratio	PP	115	161	29.5
	F1X2.5H	117	159	28.3
	F1X5.0H	116	160	32.2
	F1X7.5H	116	160	33.7
	F2X2.5H	116	160	25.4
	F2X5.0H	117	159	24.4
	F2X7.5H	118	160	31.3

This is the starting temperature of the crystallization process for a melted material and a higher T_c onset indicates an 'easiest' crystallization, namely a faster nucleation process. Although variations of this quantity are usually considered appreciable when these temperature changes are of the order of 10 °C, it is worth noting that using the higher PP-*g*-MA/cloisite ratio in "L" group shifts the T_c onset to the lower value. In the "H" group of specimens because of more limitation in the mobility of chains due to the higher degree of orientation of silicate layers, the use of higher PP-*g*-Ma/cloisite ratio would shift T_c to the higher values. Reduction in T_c for "H" group of films against "L" group is due to higher degree of orientation of silicate layers and more limitation in mobility of polymeric chains. Table 3 represents that the percentages of crystalline phase in the nanocomposite blown films, prepared with higher draw-down ratio, is lower than the group of films prepared with lower draw-down ratio. The "H" group has the faster cooling process due to its lower thickness.

This issue is notable in this work because it implies that the lower permeability of "H" group is due not only to presence of crystalline phase, but also to more orientation of silicates layers along machine direction.

3.3. Dynamic mechanical thermal analysis

As can be observed in Fig. 7 the storage modulus of nanocomposite films is higher than the storage modulus of polypropylene films. These results indicate that the glass transition temperature is lower

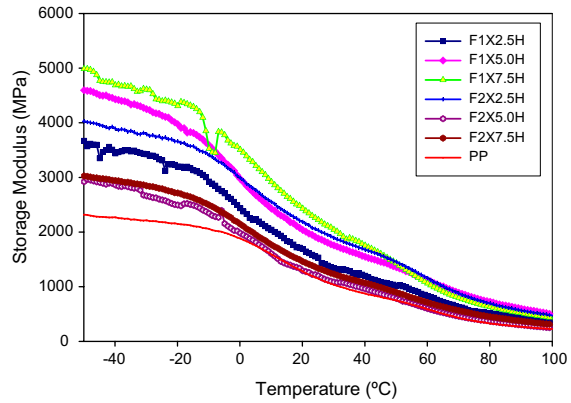

Fig. 7. Storage modulus as a function of temperature in tension mode.

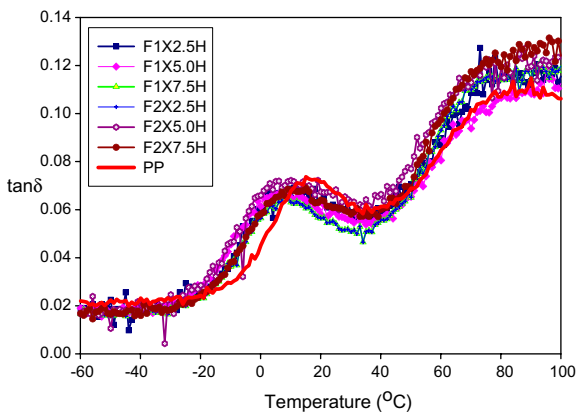

Fig. 8. tan δ as a function of temperature in tension mode.

than the temperature of permeation test, therefore these samples are in rubbery state and as mentioned earlier, the permeation behaviour can be interpreted by Henry's law and solution-diffusion model. The presence of PP-*g*-MA causes the reduction of nanocomposite glass transition temperature in comparison with the pure polypropylene films (Fig. 8).

3.4. Permeability

Table 4 represents permeability values of the films. It can be observed that the permeability of the polypropylene nanocomposite blown films is at least 1.5–2.3 times lower than pure polypropylene films. These variations can be due to the composition changes that in turn affect nanocomposite morphology and the orientation of layered silicate along machine direction.

Table 4
The permeation test results according to ASTM D1434

	Sample code	Permeability (cm^3 mil/m^2 dbar)	Diffusion coefficient (cm^2/s)	Solubility (cm^3/cm^3 bar)
Low draw-down ratio	PP	2048	2.72E−07	2.17E−02
	F1X2.5L	1349.4	1.19E−07	3.29E−02
	F1X5.0L	1085.76	8.86E−08	3.55E−02
	F1X7.5L	1176	1.01E−07	3.36E−02
	F2X2.5L	1036	8.68E−08	3.45E−02
	F2X5.0L	1216.6	1.06E−07	3.31E−02
	F2X7.5L	1068.6	8.90E−08	3.48E−02
High draw-down ratio	PP	2020	1.94E−07	3.02E−02
	F1X2.5H	1184	6.45E−08	5.33E−02
	F1X5.0H	1092	8.20E−08	3.88E−02
	F1X7.5H	880	6.66E−08	3.82E−02
	F2X2.5H	969	6.59E−08	4.26E−02
	F2X5.0H	1064	7.10E−08	4.37E−02
	F2X7.5H	967	7.06E−08	3.57E−02

3.4.1. The effect of draw-down ratio

The effect of draw-down ratio on permeability of pure polypropylene films is not remarkable. This might be attributed to the increase in the value of the solubility coefficient which lowers the effect of decreasing diffusion coefficient on the oxygen permeation. Therefore both types of oriented films show approximately the same permeability and the draw-down ratio does not have significant effect on permeation in pure polypropylene blown films.

From Table 4 it can be observed that the nanocomposite film permeability of "H" series is lower than "L" series. As DSC results indicate the samples of "H" series have lower crystallinity than "L" series, so the reduction in permeability is not due to presence of higher crystalline regions as impermeable area. These results are a consequence of more orientation of polymeric chains due to higher draw-down ratio and shear amplification [15] and more orientation in the clay platelet.

Table 4 also shows that the diffusion coefficient in "H" series is lower than "L" series. It is worth notifying that the solubility of "H" series is higher than "L" series because of existence of more amorphous regions (Table 4). Only in one of the samples (F1X5.0), the permeation does not show any variation at high and low draw-down ratios, which might be attributed to the composition of this sample leading to an excess increase in solubility factor and can suppress the barrier effect of orientation, and yet diffusion coefficient of F1X5.0H being lower than F1X5.0L. The greater change in diffusion coefficient is observed in samples containing 2.5% of cloisite and the same amount of PP-*g*-MA (F1X2.5). This might be due to lower amount of cloisite and compatibilizer of this sample which can intensify the shear amplification causing greater orientation of silicate platelets.

3.4.2. The effect of composition

The permeation of nanocomposite should be theoretically decreased by addition of organoclay due to the increase in tortuous path. However, as shown in Table 4 this trend was not observed for polypropylene nanocomposite films. The main reason for this behaviour in this nanocomposite is the presence of PP-*g*-MA. As it is known the better dispersion of nano-particles can be achieved by adding more compatibilizer but this sort of compatibilizer has also a reverse effect on permeability. It increases the diffusion coefficient of the nanocomposite due to its low molecular weight. The amount of nanoparticles and compatibilizer ratio affects nanocomposite structure. As shown in Table 4, the lower permeability is related to those samples having semi-exfoliated structure with higher degree of delamination based on XRD spectra. This behaviour shows the effectiveness of the degree of delamination on decreasing the permeability. It is found that only 2.5% of the cloisite 15A with proper dispersion and delamination caused 2.1 times decrease in permeability. If the nanoparticle with the same degree of delamination is increased by 7.5% (F2X7.5H) the permeability remains as before. This is due to the presence of 15% PP-*g*-MA in the composition of F2X7.5H. This amount of compatibilizer has significantly decreased the effectiveness of excess individual silicate platelets in the F2X7.5H in comparison with F2X2.5H.

Also in the semi-exfoliated samples (Table 2) increasing the amount of PP-*g*-MA reduces the effectiveness of draw-down ratio to orientate the silicate layers in the nanocomposite blown films so that the permeability of F1X7.5L is lower than F2X7.5L. However, due to the greater silicate layers orientation in F1X7.5 with lower amount of PP-*g*-MA, the F1X7.5H is the least permeable sample (Table 4).

4. Conclusion

The oxygen permeability coefficient decreases in nanocomposite films but the amount of this decrement is attributed to the quantity of organoclay and compatibilizer and their influence on morphology and orientation of silicate layers.

The TEM micrographs and X-ray diffraction spectra for the best impermeable samples show the coexistence of intercalated montmorillonite tactoids and exfoliated montmorillonite layers.

It is found that there is a correlation between the ratio of PP-*g*-MA/OMMT and the effect of draw-down ratio on the orientation of silicate layers which significantly changes the permeability coefficient. Increasing the amount of PP-*g*-MA reduces the orientation of silicates layers and effectiveness of these layers on increasing tortuous path.

Acknowledgements

The authors acknowledge Nanotechnology Group of New Industrials Center and the other associates for their supports of this work.

References

[1] Hirsch A. Flexible food packaging: questions and answers. Germany: Van Nostrand Reinhold; 1995. p. 28–36.
[2] Dell'Anno G. Development of a new class of hybrid reinforced thermoplastic composites based on nanoclay and woven glass fibers. PhD Thesis, Cincinnati University, USA; 2004.
[3] Manias EA, Touny L, Wu K, Strawhecker BL, Chung TC. Polypropylene/montmorillonite nanocomposites: review of the synthetic routes and materials properties. Chem Mater 2001;13:3516–23.
[4] Manias EA, Touny L, Wu K, Strawhecker BL, Gilman JW, Chung TC. Polypropylene/silicate nanocomposites: synthetic routes and materials properties. Polym Mater Sci Eng 2000;82:282.
[5] Balazs AC, Singh C, Zhulina E. Modeling the interactions between polymers and clay surfaces through self-consistent field theory. Macromolecules 1998;31:8370–81.
[6] Hasegawa N, Kawasumi M, Makoto K, Arimitsu U, Akane O. Preparation and mechanical properties of polypropylene-clay hybrids using a maleic anhydride-modified polypropylene oligomer. J Appl Polym Sci 1998;67:87–92.
[7] Benetti EM, Causin V, Marega C, Marigo A, Ferrara G, Ferraro A, Consalvi M, Fantinel F. Morphological and structural characterization of polypropylene based nanocomposites. Polymer 2005;46:8275–85.
[8] Modesti M, Lorenzetti A, Bon D, Besco S. Effect of processing conditions on morphology and mechanical properties of compatibilised polypropylene nanocomposites. Polymer 2005;46:10237–45.
[9] Bharadwaj RK. Modeling the barrier properties of polymer-layered silicate nanocomposites. Macromolecules 2001;34:9189–92.
[10] Cornelius CJ. Physical and gas permeation properties of a series of novel hybrid inorganic–organic composites based on a synthesized fluorinated polyimide. PhD Thesis, Virginia Polytechnic Institute and State University, USA; 2000.
[11] Laot CM. Gas transport properties in polycarbonate; influence of the cooling rate, physical aging, and orientation. PhD Thesis, Virginia Polytechnic Institute and State University, USA; 2001.
[12] Pukanszky B, Belina K, Rockenbauer A, Maurer FHJ. Effect of nucleation, filler anisotropy and orientation on the properties of PP composites. Composites 1994;25:205–14.
[13] Sarazin FP, Bureau MN, Denault J. Micro- and nano-structure in polypropylene/clay nanocomposites. Polymer 2005;46:1624–34.
[14] Mehrabzadeh M, Kamal R. Melt processing of PA66/clay, HDPE/clay and HDPE/PA66/clay nanocomposite. Polym Eng Sci 2004;44:1152–61.
[15] Wang K, Xiao Y, Na B, Tan H, Zhang Q, Fu Q. Shear amplification and re-crystallization of isotactic polypropylene from an oriented melt in presence of oriented clay platelets. Polymer 2005;46:9022–32.